Surface & Coatings Technology 385 (2020) 125367

Contents lists available at ScienceDirect

Surface & Coatings Technology

journal homepage: www.elsevier.com/locate/surfcoat

Cold spray deposition of solution heat treated, artificially aged and naturally aged Al 7075 powder

Alexandre Sabard[a], Philip McNutt[b], Henry Begg[b], Tanvir Hussain[a,*]

[a] Faculty of Engineering, University of Nottingham, Nottingham NG7 2RD, UK
[b] TWI Ltd, Great Abington, Cambridge CB21 6AL, UK

ARTICLE INFO

Keywords:
Al-Zn-Mg-Cu alloys
Cold spray
Microstructure
Ageing
Precipitates
Tamping

ABSTRACT

The deformation behaviour of particles and substrate in cold spray is dictated by the intrinsic properties of both materials, and their bonding directly affects the resulting properties of the deposited coating. The processing through heat treatment of aluminium alloy powders has only recently been developed for both cold spray and additive manufacturing, hence the necessity to evaluate and further understand the evolution of their properties. In this study, an Al 7075 gas-atomised powder was solution heat treated, quenched and subsequently aged. The powder in its as-quenched, T4 (natural ageing at room temperature for 21 days) and T6 (artificial ageing at 120 C for 24 h) condition was characterised through differential scanning calorimetry and scanning electron microscopy to evaluate the precipitation kinetics. Powders were cold sprayed using heated N_2 at 500 C and 6.0 MPa and the resulting deposits were evaluated using tubular coating tensile and pull-off bond strength tests. The precipitation development in the gas atomised powder was found to be similar to the bulk alloys, with development of η′ precipitates during artificial ageing and Guinier-Preston zone formation and development during natural ageing. A relationship between the deposition efficiency of the powders and the coating properties was discovered and explained through an adapted densification mechanism based on powder tamping.

1. Introduction

Developed in the 1980s in Russia [1], cold gas dynamic spray, or cold spray, is a unique thermal spray technique due to its deposition mechanism that relies on kinetic energy of particles. When introduced into a high-pressure preheated gas flow, the powder particles are accelerated and pass through a converging-diverging nozzle before they impact onto a substrate. As the particles hit the substrate, they deform plastically into splats, subsequently piling up to form a dense coating [2–4]. Due to the low working temperatures of the process, and the absence of particle melting, cold spray is a particularly suitable candidate technique for repair and part restoration [5,6], and cold spray is more advantageous over component replacement in industries such as automotive or aerospace due to cost and sustainability. Due to their ductility and high strength, aluminium alloys remain the major materials used for cold spray repair within a wide range of possible materials and applications such as magnesium castings [7], titanium hydraulic lines [8] and martensitic steel components [9].

Due to the fundamental principle of cold spray relying on kinetic energy and plastic deformation of particles, resulting coatings are often of low ductility, owing to extensive work hardening [2]. Cold sprayed precipitation-hardenable aluminium alloys can be subject to a post-spraying solution heat treatment to anneal the deposit, providing the possibility of a subsequent ageing through the development of a fine distribution of precipitates to reach optimum properties [10,11]. However, applying such high-temperature treatments to the repaired components remains undesirable in many situations. Materials such as Al and Mg are extremely sensitive to heat input, and any temperature exposure would not only affect their mechanical properties but also involve a potential distortion of the precisely machined parts. Moreover, the quenching process involved in precipitation hardening would introduce residual stress, potentially increasing the risk of stress corrosion cracking of the part. Therefore, studies have recently investigated the possibility of solution heat treating and quenching the feedstock powder prior to deposition [12–16]. These recent studies looked into homogenising the particular microstructure resulting from the powder manufacturing process, which modified the deposition behaviour of the precipitation-hardenable alloys. Depositing the heat treated powders in their as-quenched condition resulted in increased deposition efficiency and coating density for various alloys, namely Al 7075 [12], Al 6061 [13,14] and Al 2024 [14]. While the ageing of those powders was prevented in order to use them in their most ductile state,

* Corresponding author.
E-mail address: tanvir.hussain@nottingham.ac.uk (T. Hussain).

https://doi.org/10.1016/j.surfcoat.2020.125367
Received 24 October 2019; Received in revised form 9 January 2020; Accepted 13 January 2020
Available online 15 January 2020

the ageing of such alloy powders is expected to influence cold spray deposition and merits further investigation.

The ageing of precipitation-hardenable aluminium alloys is well established in common literature [17,18] and can take several forms. Following a solution heat treatment, the material is quenched and retained into a supersaturated solid solution. The material can be subsequently exposed to a low temperature heat treatment (artificial ageing) to reach optimum properties, or can remain exposed to room temperature (natural ageing), which results in more gradual evolution of strength with time [17,19]. In the case of Al-Zn-Mg-Cu (7000 series) alloys, the precipitation process is generally agreed to follow the sequence:

Solid solution → *GP zones* → η' → η

The development of solute atom clusters and precipitates determines the properties reached by the material. While natural ageing corresponds to the development of coherent clusters called GP zones, artificial ageing tends to develop a fine distribution of semi-coherent η' precipitates [20,21]. If the material is aged further, stable η precipitates can be formed. Stable η precipitates lack coherency with the aluminium matrix and their development in the material induces a loss in material strength and an increase in ductility [19]. While the effect of precipitates within the sprayed particles upon impact on a substrate is still to be discovered, recent studies investigated the effect of second phases within Cu particles [22]. It was reported that these second phases act as a nucleation site for recrystallisation within the powder during the severe plastic deformation, also affecting the compression ratio of the Cu particles. While a distribution of strengthening precipitates corresponds to a different scale and size of secondary phases, the powder ageing is believed to have an influence on its cold spray potential through the variation in powder strength and ductility.

As aluminium alloy powder heat treatment has only been recently developed for cold spray [12–15] and additive manufacture [23–25], it is necessary to investigate the evolution of this material upon ageing prior to deposition. In this study, the artificial and natural ageing of a solution heat treated Al 7075 powder was investigated by differential scanning calorimetry (DSC) and scanning electron microscopy (SEM). The processed powders were subsequently cold sprayed, and the resulting coatings were characterised through bond strength tests as well as tubular-coating-tensile tests to study the mechanical properties.

2. Experimental methods

2.1. Materials

A spherical gas-atomised Al 7075 powder with composition 0.2 wt% Si, 2.5 wt% Mg, 0.2 wt% Fe, 1.6 wt% Cu, 0.2 wt% Cr, 0.01 wt% Ti, 0.05 wt% Mn, 5.8 wt% Zn, bal. Al (TLS Technik, Germany) was used to perform cold spray deposition. The Dv_{10}, Dv_{50} and Dv_{90} were respectively measured at 31.5, 48.5 and 73.1 μm. Coatings were applied onto 5 mm thick 7075-T6 aluminium alloy plates for microstructural analysis and onto 7075-T6 30 mm-diameter discs of 5 mm thickness for adhesion testing, while coatings were deposited onto 25.4 mm diameter commercially pure Al dollies for tubular-coating-tensile (TCT) testing [26].

2.2. Solution heat treatment and processing of the powder

A box furnace (Carbolite, Sheffield, UK) was modified in order to be used as heat treatment facility under inert atmosphere. A stainless steel vessel, made of two parts joined by a flange and sealed by a compressed copper gasket, contained the powder. The 160 mm-diameter vessel was rotated at 36 rpm in order to avoid sintering. Ar was used as a shielding gas during the process at a constant flow of 4 l/min, keeping the vessel pressurised at 0.1 MPa. The facility is represented in Fig. 1. Following the heat treatment cycle, an Ar gas flow was flown through the vessel at 70 l/min to evacuate it to the quenching apparatus, cooling it down rapidly. The powder particles were subsequently separated from the gas by a cyclone. The as-atomised powder was solution heat treated at 475 °C for 1 h and quenched. Quenching rate was not directly measured but was assumed to be sufficient for homogenisation based on microstructural analysis. The temperature was chosen following the standard precipitation heat treatment procedure of Al alloys [19].

2.2.1. Solution heat treated and quenched (SHT)

In order to prevent the as-quenched powder from ageing, the as-quenched powder was kept in a freezer stabilised at −70 °C. The particles remained in the facility for 96 h before cold spraying.

2.2.2. Naturally aged powder (T4)

A batch of the as-quenched Al 7075 powder was exposed to room temperature for 21 days in order to allow natural ageing. The ageing time was chosen based on preliminary studies covering the ageing behaviour of Al-Zn-Mg-Cu alloys at room temperature, in order to provide enough time for the powder hardness to reach a plateau. This statement is based on previous experiments, where a batch of solution heat treated, and quenched Al 7075 powder was left at room temperature and its hardness was measured daily. From 81 HV0.1, the hardness increased to 149 HV0.1 after 16 days, and no further increase was measured subsequently during the next 10 days.

2.2.3. Artificially aged powder (T6)

In order to artificially age the powder, a batch of as-quenched Al 7075 was inserted in a stainless steel flask filled with Ar. The powder was heat-treated at 120 C for 24 h following a heating rate of 10 C/min in a box furnace, following the standards for a T6 heat-treatment of Al 7075 alloy [18] and was subsequently cooled down by removing the flask from the box furnace.

2.3. Cold spray deposition

The coating deposition was performed using Impact Innovation 5/11 and N_2 as a primary gas. The N_2 pressure and temperature were maintained at 6.0 MPa and 500 C throughout the cold spray deposition, based on previous parameter optimisation trials. The parameters were selected based on the density and deposition efficiency of the coatings resulting from the trials. The deposit thickness was kept consistent between 300 and 350 μm by varying the number of passes onto a substrate ground with P120 silicon carbide paper. The standoff distance was maintained at 30 mm and the number of passes was varied to obtain a 350 μm coating. 9 passes were sprayed for the SHT powder, 22 for the T4 powder and 53 for the T6 powder for all tested samples including bond strength and TCT. A scanning speed of 500 mm/s was used during the spray runs, with a track spacing of 1 mm. 3 samples were sprayed of each powder for microstructural characterisation, 5 for bond strength tests and 3 for TCT testing. Swipe tests were sprayed in one pass, at a scanning speed of 2000 mm/s in order to analyse individual particles, where the substrate was ground with P600, P1200 and P2500 silicon carbide paper, and subsequently polished using 3 and 1 μm diamond suspension to reach a mirror-like surface.

2.4. Microstructural characterisation

The powder and coatings cross-section microstructures, as well as the fracture surfaces were observed using a field-emission gun SEM (SIGMA, ZEISS, Germany) operating at 20 kV in both secondary imaging (SE) and backscattered electron (BSE) modes at a working distance of 8 mm. All the samples were sectioned using a precision saw at a cutting speed of 0.005 mm/s. The powders and cross-sectioned coatings were mounted in epoxy resin and ground with P600, P1200 then P2500 silicon carbide paper. They were then sequentially polished using 3, 1 and 0.25 μm diamond suspension. Final polishing for high-resolution

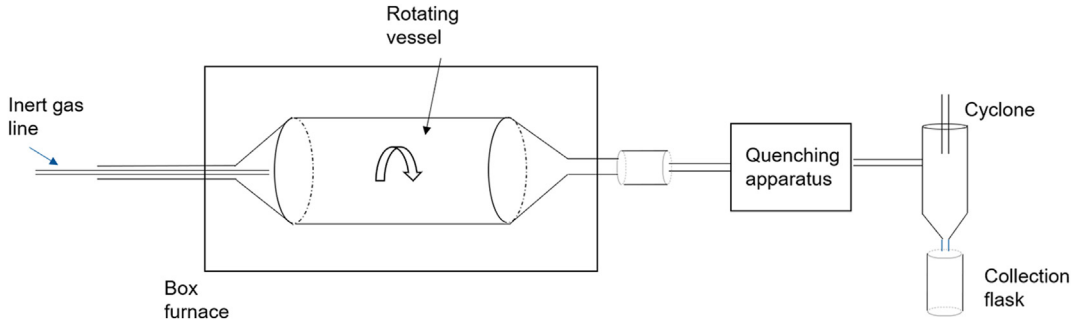

Fig. 1. Inert atmosphere heat treatment facility used for powder processing.

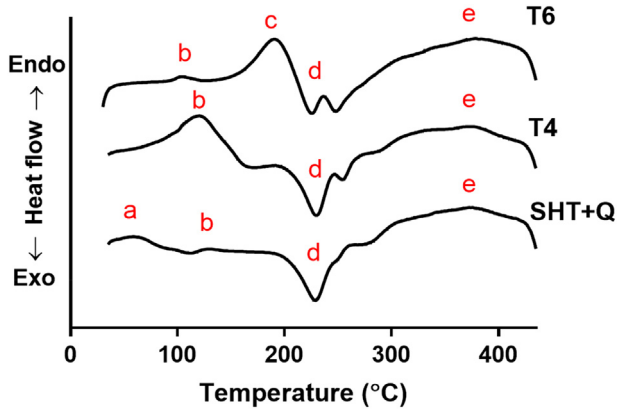

Fig. 2. Differential scanning calorimeter graphs of Al 7075 powder in different conditions. Major differences between powders were observed at low temperatures (50–200 °C), as endothermic peaks appear shifted towards higher temperature with ageing.

imaging was performed using a colloidal silica (0.05 μm) suspension. Fracture surfaces were observed by inserting the pulled dollies in the SEM chamber.

The aluminium powder was characterised using DSC with a DSC 4000 (Perkin Elmer, MA, USA) by heating from room temperature to 450 C at a rate of 10 C/min. 50 mg of powder were inserted in aluminium pans, of which the signal was subtracted to obtain the thermogram of the powder itself. Shielding gas was N_2 during the experiments, and due to the relatively low temperature reached during the thermal analysis cycles, no reaction occurred between the powder and N_2. Samples were also cooled at 10C/min, but the results issued from the cooling are not included in this manuscript.

2.5. Microhardness measurements

Microhardness measurements of the powders and coatings were performed on an MMT-7 Vickers Microhardness instrument (Buehler, USA), with a 10-gf (0.1 N) load and 10 s dwell on the polished cross-section. 8 measurements were performed, and the mean values reported. Indents were located in the centre of the coatings.

2.6. Adhesion tests

The bond strength of the aluminium alloy coatings onto the aluminium alloy substrates was measured according to ASTM standard C633-01 [27]. The coating was deposited onto 28 mm diameter flat discs, which were ground with P120 grit paper before being sprayed onto. The back of the substrate was grit-blasted, as were the steel dollies that were glued onto each side of the sprayed samples. A room temperature curing adhesive (Scotch Weld DP270 (3M, UK)) was used to minimise unwanted ageing effects and enable full curing strength to be reached within 24 h.

Each powder was sprayed onto 5 different samples. Once glued, the samples were turned down to 25.4 mm and adhesion strength measured in a servo-hydraulic tensile testing machine, at a rate of 1 mm/min.

2.7. Tubular tensile coatings testing

In order to obtain data about the cohesive strength of the coating, Tubular Coating Tensile testing (TCT) [26] was performed on the coatings. Two cylindrical Al dollies (25.4 mm diameter) were installed facing each other on a rod. Once held in place, the dollies were slightly turned down to ensure their alignment. A lathe rotated the samples at 370 rpm, while the nozzle transverse speed was set to 6.17 mm/s corresponding to a lateral movement of 1 mm after each rotation. 3 samples were tested for each powder condition.

Once deposited, the dollies were tested in a servo-hydraulic tensile testing machine at a rate of 1 mm/min. The resulting cohesion strength was multiplied by a correction factor equal to 1.5 due to a stress concentration factor at the boundary between the two dollies [26].

3. Results

3.1. Characterisation of solution heat treated and quenched Al 7075 powder

The DSC graphs corresponding to the powders in various conditions are shown in Fig. 2. Four different endothermic peaks can be observed in the thermogram and are labelled ***a***, ***b***, ***c*** and ***e***. The peak labelled ***d*** corresponds, however, to the only exothermic peak present in the DSC scans of those Al-Zn-Mg-Cu alloys. The presence of these peaks and the variation in heat flow generally agrees with the previous studies performed on similar alloys [28–31]. From the precipitation sequence of Al-Zn-Mg-Cu alloys and the previously reported literature [28–33], it is possible to suggest the phases responsible for these heat flow variations. Peaks ***a*** and ***b*** correspond to the formation of clusters and GP zones respectively. The distinct peak ***c*** is however a sign of dissolution of η′ precipitates [29,30], corresponding to the strengthening precipitates of typical Al 7075 alloys. The doublet peak ***d*** corresponds to further formation of these metastable precipitates η′, and the formation of its stable version, η. Finally, the large endothermic peak ***e*** is generally agreed to be representative of the dissolution of η′ and η.

Table 1 summarises the precipitation evolution and the corresponding peaks.

The peaks of interest, and the main differences in the powder behaviour can be observed in the first endothermic peaks ***a*** and ***b***. The solution heat treated and quenched powder (SHT + Q) exhibits only small peaks corresponding to a minimal number of clusters formed. Despite attempting to prevent any ageing from occurring, it was impossible to prevent the material to be exposed to room temperature during the whole process, and a few clusters and precipitates corresponding to GP zones have been formed and are dissolved in the early

Table 1
Peak identification associated with the DSC results Fig. 2 and the corresponding temperature.

	a	b	c	d	e
SHT + Q	Clusters dissolution 54 °C	GP dissolution 120 °C	…	η′/η formation 223 °C	η dissolution 300–420 °C
T4	…	GP dissolution 111 °C	…	η′/η formation 225 °C	η dissolution 300–420 °C
T6	…	GP dissolution 103 °C	η′ dissolution 192 °C	η′/η formation 218 °C	η dissolution 300–420 °C

stages of the thermal cycle.

The main differences between the heat treated powders are located in this low temperature range. The T4 powder, having undergone a natural ageing of a few weeks, presented a large increase in peak amplitude at 120 °C, corresponding to the dissolution of GP zones (peak ***b***). The formation of GP zones during natural ageing has been widely studied [21,34,35] and the strengthening of the material in the early stages of the ageing has been attributed to the presence of those species, and their coherence with the Al matrix.

The artificially aged or T6 powder presented different heat flow variation in the same temperature range. While peak ***b*** exhibited a low amplitude at 110 °C, a large peak ***c*** was observed at 190°. Attributed to the dissolution of strengthening precipitates η′ [29,30], it highlights the ageing process undergone by the particles. According to previous studies on the ageing process of Al-Zn-Mg-Cu, artificial ageing of aluminium alloys is associated with the homogeneous growth of a fine distribution of meta-stable precipitates, providing the required strength by interacting with the aluminium matrix [36,37].

While the dissolution of η′/η precipitates corresponding to peak ***e*** on the thermograms does not seem to be greatly affected by the ageing state of the Al 7075 powder, the second peak of the doublet ***d*** increased with the ageing time and temperature. While almost absent in the as-quenched condition, its enthalpy increased in the naturally aged condition, reaching an even higher value for the artificially aged powder. This phenomenon can be explained through nucleation and precipitate growth. While the as-quenched material is relatively free of precipitates, as it remained not exposed to room temperature, both aged powders happen to be in an advanced precipitation stage at the beginning of the thermal analysis. The existing precipitates act then as precursors or nuclei for the next phases developed, namely η and η′ [20], increasing their number once the material reaches a sufficient temperature.

The cross-section of the powders after SHT + Q, SHT + Q + natural ageing, SHT + Q + artificial ageing is presented Fig. 3. The low magnification images revealed no major difference in the microstructure, as all three appear similar. A few remaining precipitates can be distinguished in the particle's microstructure; however, the dendritic structure, typical of a gas-atomised aluminium alloy [38] (not shown here) has been dissolved by the heat treatment performed in this study. High-magnification micrographs revealed a fine distribution of precipitates in the T6 powder microstructure, distinguished by their bright contrast compared with the grey aluminium matrix. This particular microstructure can be correlated with the presence of peak ***c*** in the DSC results presented Fig. 2. Through peak-ageing, a fine distribution of η′ precipitates was developed in the powder microstructure and was dissolved in the early stages of the thermal analysis. No clear difference was, however, observed between the naturally aged powder (T4) and the as-quenched one. This was attributed to the limitation of the imaging technique.

3.2. Cold spray deposition

In order to understand the effect of the powder processing on its ability to deform during cold spray, swipe tests were performed. By cold spraying the different powders onto a similar substrate at high scanning speed, individual particle impacts were examined. The tilted view (70°) images of the powder particles revealed differences in deformation behaviour (Fig. 4). Micrographs of the as-quenched powder, having undergone no ageing, suggested the deformation was largely confined to the incident particle, inducing a large amount of deformation that resulted in cracks on the outer edges. Conversely, both T4 and T6 powders showed a deeper anchoring in the substrate and no edge cracking. The increase in strength provided by the ageing (natural or artificial) appeared to enable a more equal distribution of strain between particle and substrate. Jetting was observed on the edges of the T6 particle, coming from the substrate rather than the incident particles as indicated by the black arrow (Fig. 4).

Coating deposition was performed for the three different powders and the cross-sections of the resulting deposits are shown in Fig. 5. The as-quenched powder exhibited higher porosity and voids were observed in the coating microstructure. It was also noted that the coating appeared to be delaminated from the substrate and a slight gap was observed between the coating and the substrate, indicating weaker adhesion. The coating sprayed using T4 powder exhibited lower apparent porosity (Fig. 6), with no evidence of voids present in the deposit microstructure, suggesting a good bond between particles. The coating sprayed using T6 powder exhibited a higher porosity than the T4 samples and a higher volume fraction of defects/voids.

While solution heat treated and quenched powders exhibited the highest level of porosity, the deposit efficiency of the coating process was also the highest at 25%, compared with only 10% and 6% for T4 and T6 respectively.

The microhardness of both powders and coatings is reported in Table 2: Microhardness values in HV0.1 of the powder particles as well as the coatings measured using 8 indents. The effect of ageing and the influence of precipitate structures is evident, with hardness increasing from 81.1 HV0.1 for as quenched powder to 176.1 HV0.1 for the artificially aged powder. The fine distribution of precipitates observed in the particles' cross-section induced the largest hardness increase during ageing. Ageing at room temperature also resulted in an increase in hardness, with the Al 7075 powder hardness having increased to 150 HV0.1 during the process. While not readily apparent in the SEM images, this result supports the hypothesis that GP zones were formed during the natural ageing process. The formation of clusters at room temperature has been reported in Al-Zn-Mg-Cu alloys and is held responsible for increases in material strength over time through precipitation hardening [17]. While peak strength is not reached due to the nature and the size of the clusters, it provides a significant increase in material properties such as hardness [20].

The hardness of the coatings is also reported in the same table and illustrates the work hardening occurring during deposition. The largest increase in hardness reported corresponds to the as-quenched powder, observing a 75% increase upon deposition. However, both aged powders, having a relatively high hardness before deposition, show a much lower increase in hardness of approximately 20%. This suggests that the enhanced deformability of the SHT + Q powder increases the work hardening occurring in the powder particles despite an overall lower porosity in the resulting coating.

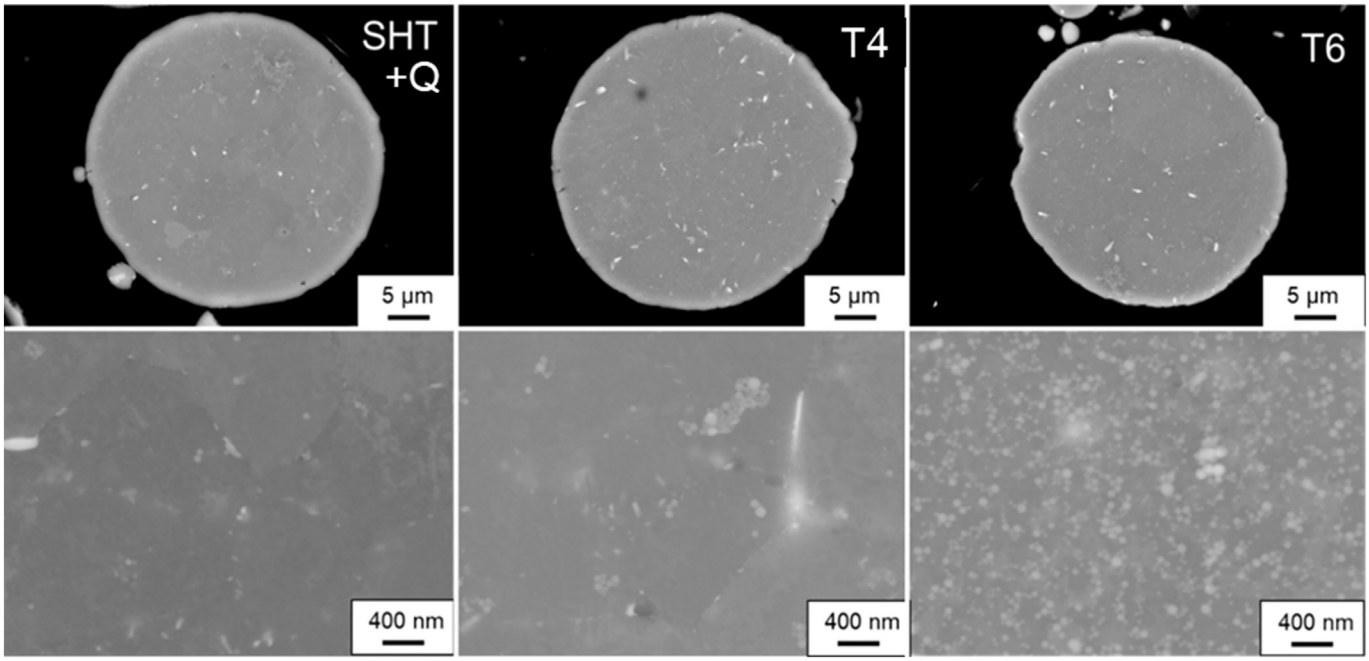

Fig. 3. BSE cross-section of the Al 7075 in various ageing conditions. No difference was observed at relatively low magnification, while a fine distribution of precipitates was observed at higher magnification in the case of the artificially aged powder.

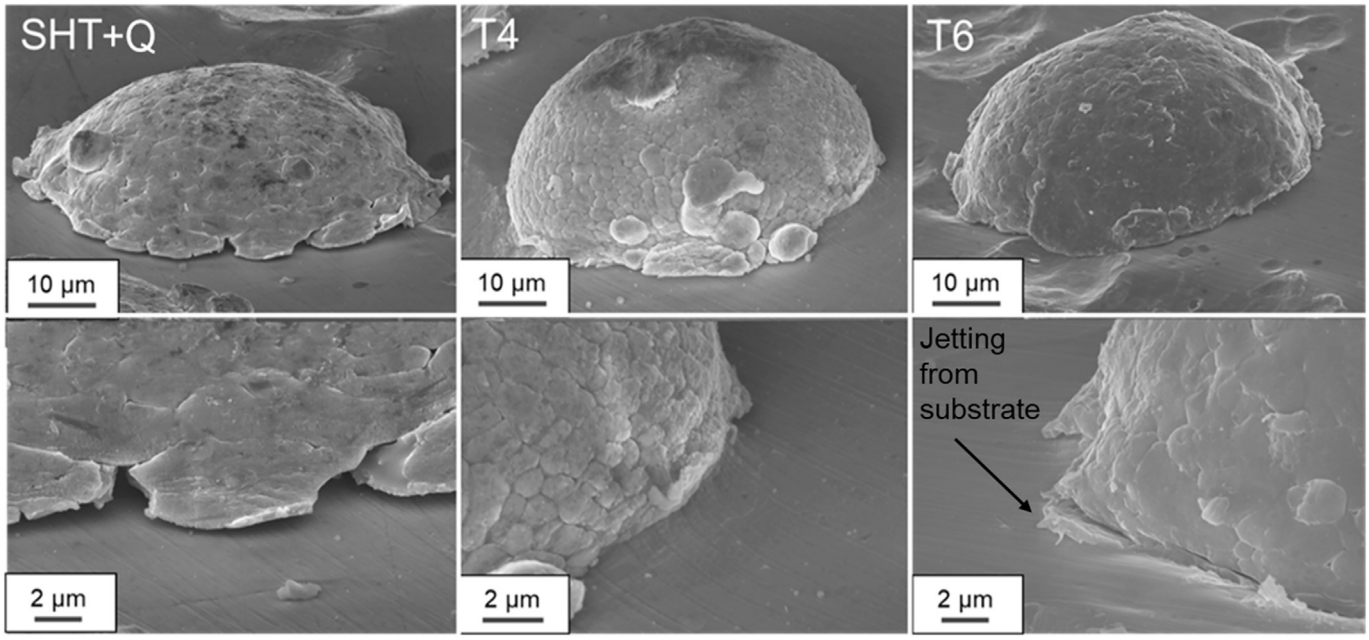

Fig. 4. Tilted SEM images (70°) of particles sprayed onto an Al alloy substrate showing their interaction with the material upon impact. Black arrow indicates jetting coming from the substrate.

3.3. Testing of cold sprayed coatings

Adhesion testing showed that coatings produced from SHT + Q powder resulted in a low bond strength (Table 3), while both coatings produced from aged powder failed in excess of the glue strength. The limitation of the test procedure prevented the true bond strength of the T4 and T6 samples from being measured. The adhesive failure was measured at two different loads, fact attributed to a potential variation in the application of this adhesive.

However, TCT cohesion testing does not require the use of adhesives and can provide valuable information on the mechanical performance of all three coatings. A clear increase in coating cohesion was exhibited by both coatings sprayed using the aged powder (T4 and T6) (Fig. 7). The SHT + Q powder coating showed a low cohesion value of 220 MPa, whereas the T4 and T6 powder coatings were measured at 400 MPa and 500 MPa respectively. Despite remaining lower than the bulk values, such cohesion strength highlights the effect of the powder characteristics on the resulting coating properties.

Fractographic examination of the TCT surfaces revealed two different morphologies (Fig. 8). The first one being represented by red arrows, corresponds to smooth surfaces typical of particle-particle rupture. A particle decohesion requires less strain and tends to suggest brittle behaviour. The second morphology is indicated by the white arrows and suggests fracture by likely void coalescence. Typically

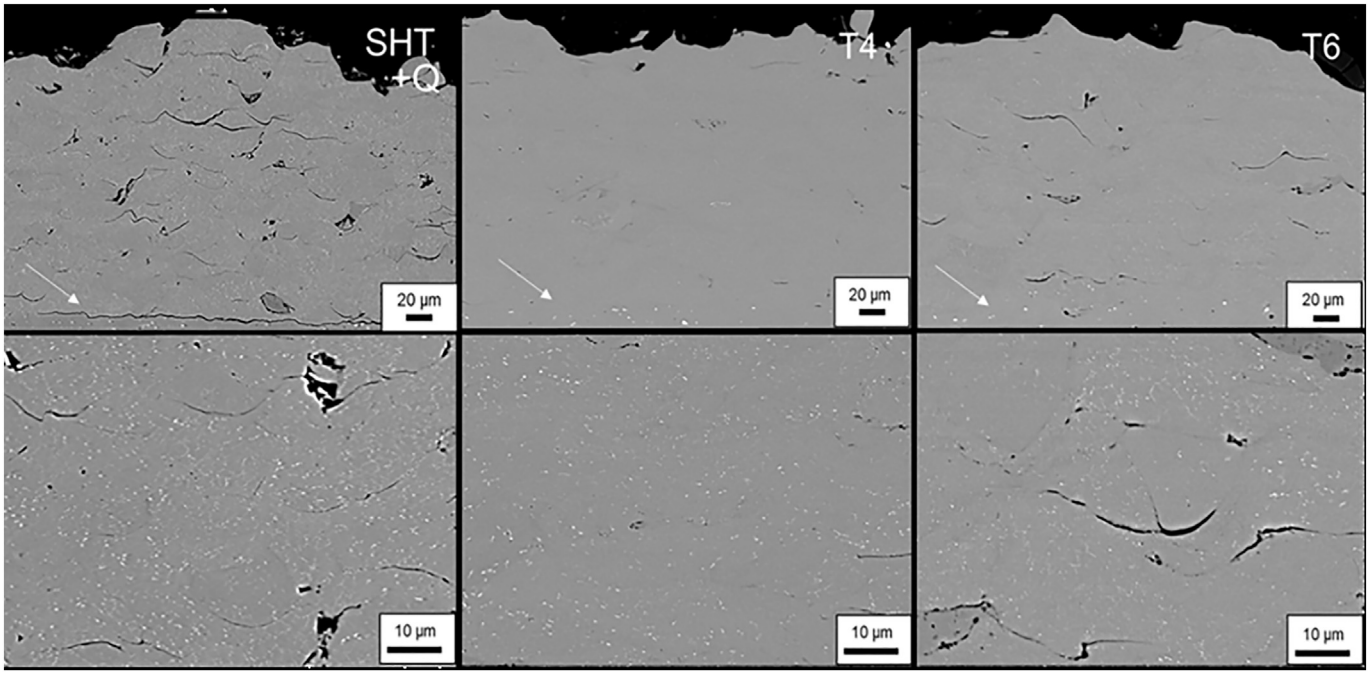

Fig. 5. Cold sprayed Al 7075 microstructure in cross-section. Top images show the lower magnification including the substrate/coating interface, and lower images indicates the higher magnification micrographs. Coatings were sprayed until they reached 300 µm for consistency in mechanical testing. Interfaces between the substrate and the coating are indicated by a white arrow in all cases.

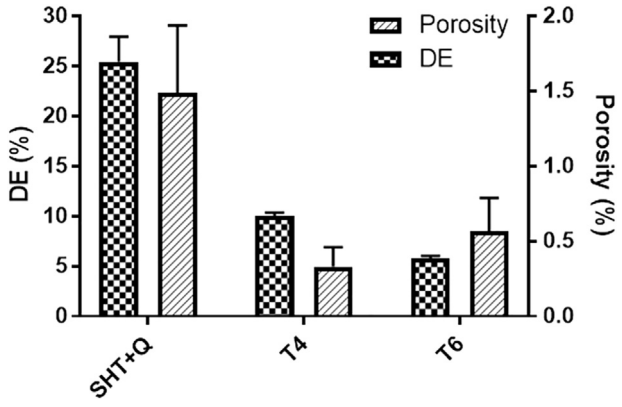

Fig. 6. Graph representing the deposition efficiency (DE) and the porosity for the different powders used in that study. The SHT + Q powder, deposited with a higher efficiency, exhibits a relatively high level of porosity compared to the aged powders.

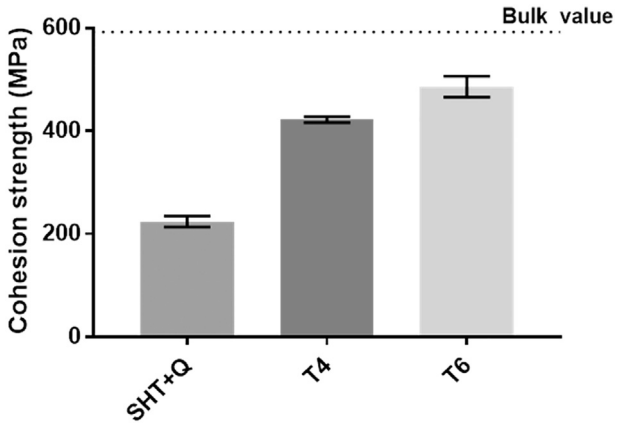

Fig. 7. Cohesion strength of the coatings sprayed using an Al 7075 powder with different degrees of ageing. A gradual increase in cohesion strength is observed with ageing. Measured values were 224 MPa (SHT + Q), 422 MPa (T4) and 486 MPa (T6).

Table 2
Microhardness values in HV0.1 of the powder particles as well as the coatings measured using 8 indents.

Microhardness (HV0.1)	SHT + Q	T4	T6
Powder	81.1 ± 4.2	149.6 ± 6.5	176.1 ± 5.6
Coating	142.2 + 10	178.8 + 6.9	205.1 + 8.2

Table 3
Adhesion values of the various coatings tested following ASTM C633. Both aged powders (T4, T6) samples failed within the adhesive.

Sample	Failure mode	Bond strength (MPa)
SHT + Q	Adhesion	11.1 ± 2.2
T4	Adhesive failure	In excess of 54.9
T6	Adhesive failure	In excess of 62.3

illustrated by the presence of dimples, it suggests ductile behaviour. While the SHT + Q powder coating mainly failed due to particle decohesion, the T4 powder coatings appeared to present a mixture of particle-particle rupture and ductile tearing. The T6 powder coating was, however, covered with dimples, suggesting a fracture occurring mainly in a ductile manner.

In order to further examine the fracture mechanisms of the deposits on a microstructural level, the TCT samples were cross-sectioned and prepared for metallographic analysis. The etched microstructure of each coating is displayed (Fig. 9). Indicated by yellow circles, entire particles can be observed at the interface, suggesting that the rupture occurred along the particle-particle boundaries. The aged powder coatings presented a different behaviour. As indicated by yellow arrows, most particles at the interface appear torn and appear to have been pulled during the test, leading to an ultimate fracture once the local stress exceeded the strength of the particles. In the absence of a

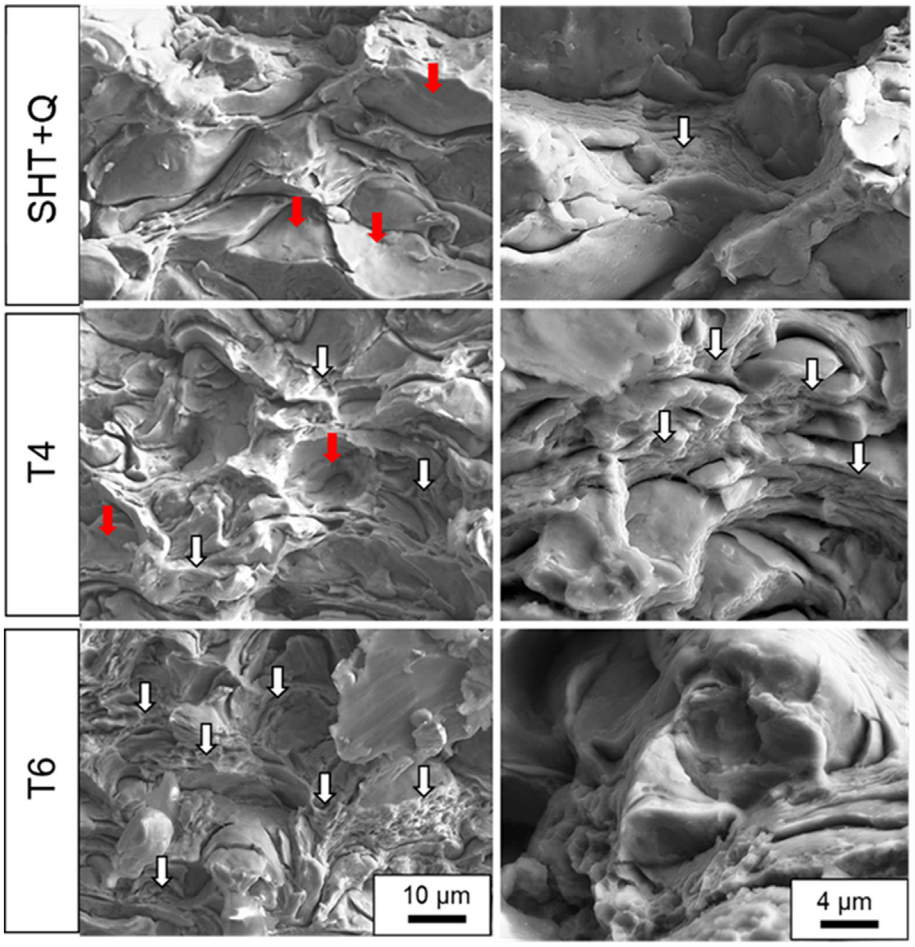

Fig. 8. Fracture surfaces of TCT samples for the different studied coatings (SHT + Q, T4, T6). As red arrows indicate the sign of particle debonding, white arrow show the signs of intraparticle ductile failure. (For interpretation of the references to colour in this figure legend, the reader is referred to the web version of this article.)

weak path for a rupture due to a good inter-particle bonding, the particles themselves were pulled, until fracture. This highlights the strong cohesion within the deposit and suggests a coating with satisfying properties.

Fig. 10 presents the top surface view of the different studied coatings, at relatively low and higher magnification. While peening

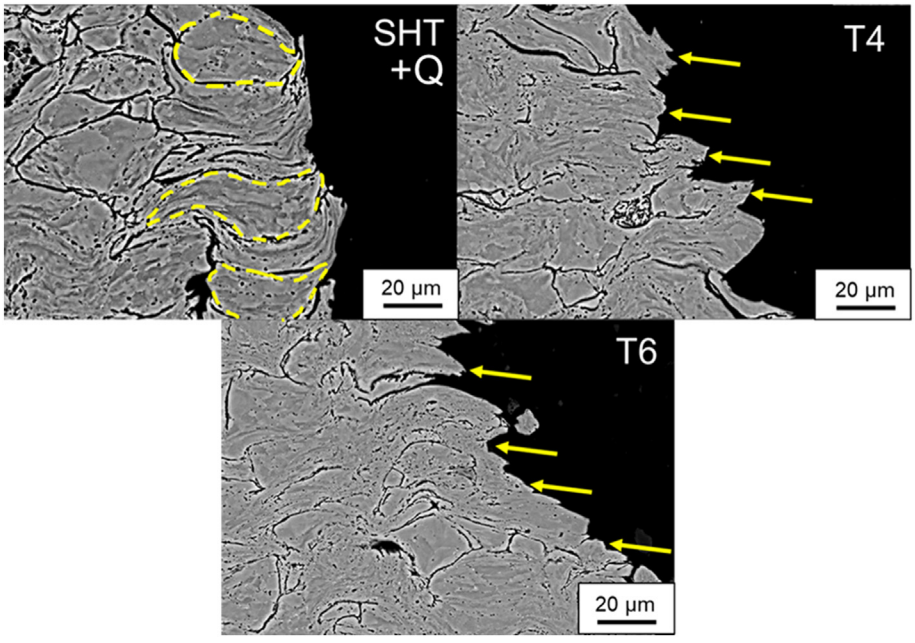

Fig. 9. Cross-section of fractured TCT dollies, considering the force applied during testing was from right to left. Yellow arrows highlight the areas of particle tearing, while yellow circles show the entire particles remaining at the fracture interface. (For interpretation of the references to colour in this figure legend, the reader is referred to the web version of this article.)

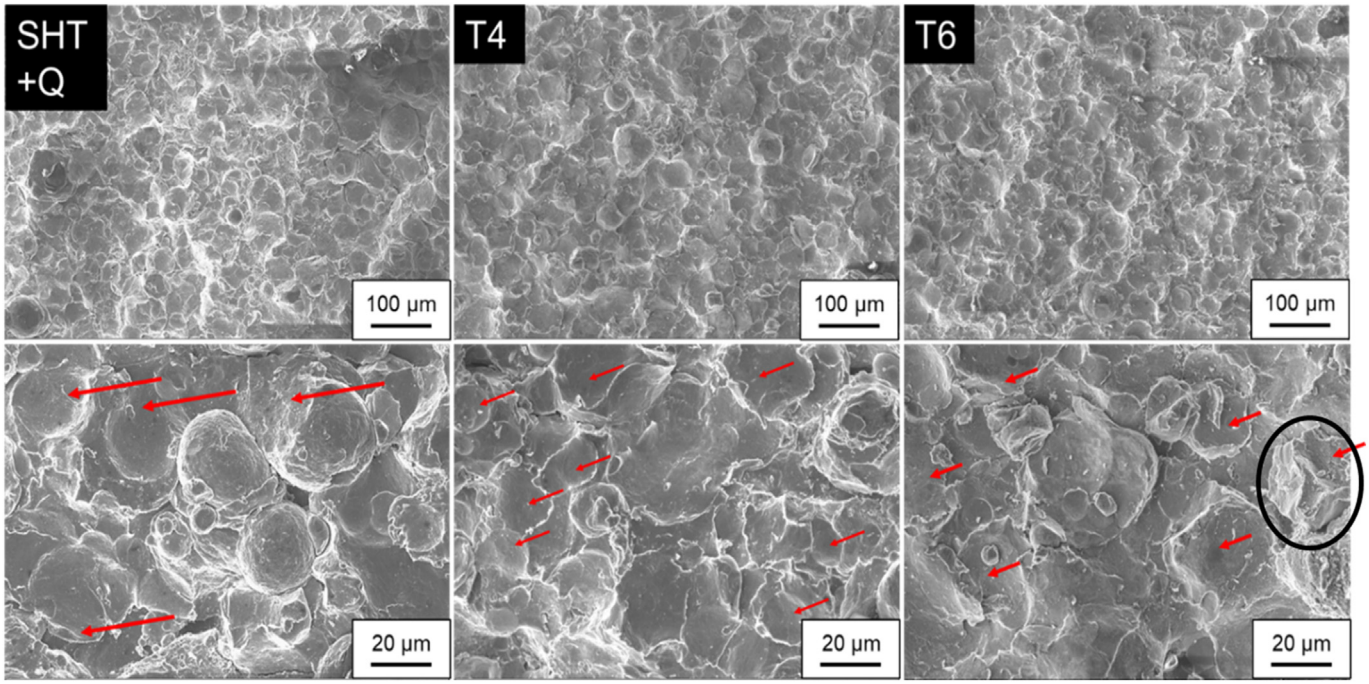

Fig. 10. Top-view of the surface of the coatings sprayed with different powders. Top line corresponds to low magnification, whereas bottom line is higher magnification images of the various coatings. Red arrows indicate peening artefacts, and the black circle indicates a particle showing impact traces on various sides. (For interpretation of the references to colour in this figure legend, the reader is referred to the web version of this article.)

artefacts are observed across all coatings, indicated by red arrows, clear differences remain in the aspect of the top surfaces. Few spherical particles remain at the top surface of the SHT + Q coating, appearing untouched by any potential peening. On the other hand, only a few remaining particles can be distinguished on both aged coatings. Both sprayed with extremely low deposition efficiency, the ratio of bouncing particles was such that it "annihilated" the surface, as highlighted by the particle in the right-hand side of the high magnification T6 top image, circled in black in Fig. 10. This particle, still present within the deposit, was compressed and damaged on several sides.

4. Discussion

4.1. Ageing behaviour of aluminium alloy powder

The importance of the powder properties in cold spray deposition has been widely covered over the last years in parallel with the development of the spraying technique itself [39–41]. In absence of melting during the coating deposition process, controlling the properties of the incident particles is crucial for any coating development. Due to their precipitation-hardenable nature, solutionised aluminium alloys have the possibility to be microstructurally modified by applying a relatively low temperature heat treatment (i.e. ageing). As recent studies discovered potential improvement in cold spray deposition by pre-processing the feedstock powder through a solution heat treatment [12–15] or a simple degassing [16], this study covers their behaviour upon spraying in different ageing conditions. As the solution heat treatment of aluminium powder remains an operation that has to be done in specific conditions due to the reactive nature of the material, only a limited number of studies have been reported on this specific topic. Hence, the behaviour of aluminium alloys powder upon ageing has not been yet covered.

As precipitates in aluminium alloys are mostly nanometric features not readily resolved by SEM (from < 1 nm in the early stages to 5–6 nm in the later stages of ageing [20]), DSC was employed to aid microstructural understanding. The thermogram of the SHT + Q powder is in general agreement with previous data reported on a similar material in its bulk form [28]. By keeping the powder not or barely exposed to room temperature, ageing was minimised and only a few clusters were characterised in the SHT + Q powder. It did not result in major hardness changes as values as low as 80 HV0.1 were measured from the as-quenched powders. On the other hand, naturally aged (T4) powder exhibited a large increase in hardness, as the sole fact of exposing the material to room temperature for 3 weeks resulted in a nearly 90% hardness increase (from 80 to 150 HV0.1). Attributed to the development of GP zones within the material as suggested by thermal analysis, it has nonetheless not been confirmed by the microstructural observation (Fig. 3). This observation generally agrees with typical GP zones development within bulk material. Characterised using transmission electron microscopy (TEM) in several studies, the atom clusters were only measured up to 2–3 nm [21,34], and such nanometric features can hardly be detected through SEM. A more substantial hardness increase was observed in the artificially aged powder, and values as high as 176 HV0.1 were measured. By heating the powder particles to 120 °C, the development of semi-coherent η′ precipitates, as suggested by DSC analysis (Fig. 2) was such that they were characterised through BSE imaging. Appearing to be around 40–50 nm in size, it corresponds to larger precipitates as compared to the typical 10–20 nm η′ observed in alloys in similar ageing conditions [42], suggesting a different behaviour between gas-atomised powder and bulk alloys. Due to a large specific surface area, and thus a shorter soaking time, each individual powder particles experience a quicker rise of temperature as compared to larger bulk material. Particles then reach the temperature required for the diffusion to begin within the matrix earlier, hence precipitates possibly forming earlier on in the ageing process.

The phase composition and microstructure of the powder particles then ultimately influence the hardness and mechanical properties, thus having an effect on cold spray deposition. The relative hardness of the powder with respect to the substrate can change the mechanism by which cold spray deposition occurs. In this study, we observed that the ageing, natural or artificial, modified this interaction. Bae et al. [43] used a thermo-mechanical model to highlight the different mechanisms occurring depending on which of the materials would be the soft counterpart. As the as-quenched powder remains in a soft state before

deposition, a clear soft/hard interaction is observed (Fig. 4). The major part of the deformation occurs within the incident particle, leading to fracture of the particle at the edges. Cracks were evident on the outer rim of the aluminium powder, potentially following the precipitates distribution along the grain boundaries that can be observed on Fig. 3. The higher strength of the aged Al powders induced different behaviour during deposition, with a more spherical shape kept by the particle, suggesting a deeper penetration in the substrate.

4.2. The importance of peening in cold spray deposition

The tendency of aluminium alloys to age at room temperature at a relatively fast rate is unique to only a few materials and its effect on cold spray deposition was still yet to be fully understood. However, the present study has shown clear differences in behaviour between Al powders in differently aged conditions deposited by cold spray, with deposition efficiencies of 25% and 6% for soft (81 HV0.1) SHT + Q powder compared with hard (176 HV0.1), T6 powder. The resulting mechanical properties of the deposit also exhibit significantly different behaviour, with a five-fold increase in adhesion strength and a doubling of the cohesion strength between SHT + Q and T6 powders. The reasons for such increase are potentially numerous. However, it remains relatively counterintuitive that the softer powder, depositing in a much more efficient way, results in a more porous, weaker coating. Ductility is often considered as a critical property in cold sprayed deposit and a particle's ability to deform upon impact is often modified through process parameter optimisation, or through additional processes such as the implementation of a laser heating the surface.

A recent study reported a similar trend in deposit efficiency and coating hardness by spraying CP (Commercially pure) Al coatings at various particle velocities [44]. As the particle velocities increased from 600 to 750 m/s, the coating density decreased. This density then increased when velocities increased from above 800 to 1000 m/s, by using He as the process gas.

This mechanism was simply described by using an energy balance equation, expressed using the following terms [44]:

$$E_{total} = E_{primary} + E_{secondary}$$

with $E_{primary}$ being the plastic dissipation energy of the particle itself during impact, while $E_{secondary}$ corresponds to the plastic dissipation energy caused by later incoming particles impacting the already-deposited particle. This effect is referred to as 'tamping' or 'hammering' and can result in coatings where lower layers exhibit higher density than more porous upper layers. At lower velocity, DE is low, and a greater number of particles rebound without bonding. This can lead to a greater tamping effect and result in higher apparent density. As velocity is increased, DE increases and fewer particles rebound. This leads to less tamping and, counterintuitively, an increase in porosity.

All powders in the present study were deposited under nominally the same conditions and therefore all particles were considered to have similar impact velocities. However, their differing hardness results in differences in deposition efficiency. As DE decreases with ageing, the number of rebounds and the degree of tamping increases, leading to a densification of the coating. Such effects can be considered to account for the observed differences in both porosity and mechanical properties. Only a few options are although available to evaluate and observe effects such as peening and tamping in the deposits. One possible option is to characterise the top-surface of the resulting deposits and investigate signs of this phenomenon through the particle's deformation and the presence of particle impact signs. Fig. 10 provides the visual signs of this hammering of incident particles. When several particles remain untouched at the top of the SHT + Q coating, both coatings sprayed using aged powders exhibit signs of tamping all over their top-surfaces.

Fig. 11 illustrates the relationship between coating cohesion strength and DE. The values corresponding to the feedstock powder (before any thermal processing) are included for comparison. A clear linear trend is observed, where the coating strength appears to be negatively correlated with the DE. The compression occurring during the deposition of coatings due to a lower DE, increases the overall strain in deposited particles and appears to increase the particle-particle cohesion. Cohesion between the particles was such that fracture happened through the particles in the cases of the aged powder coatings, as revealed by the TCT tests cross-sections (Fig. 9).

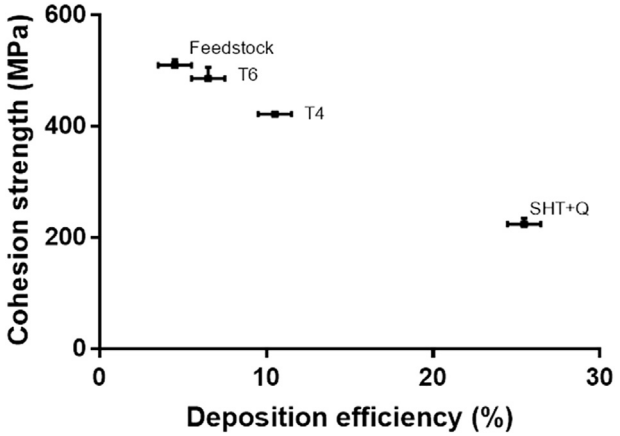

Fig. 11. Relationship between coatings cohesion strength and powder deposition efficiency for various ageing conditions.

Despite the microstructural modifications, it appears that the main factor involved in cold spray deposition in this study was the DE. It is however important to notice that, in order to compare coatings of similar thickness, the number of passes required for each coating was different, affecting greatly the deposition conditions. While ageing of the powder modified the interaction of the incident particles with the substrate, the reduction in DE induced by the associated hardness increase was considered to be the primary factor influencing mechanical properties. Through the increase in particle strength provided by precipitation hardening, the kinetic energy required to deform the particles increased. As the spraying conditions remained identical throughout the study, powder particles were hitting the substrate at the same velocities, and their different intrinsic properties resulted in a variation in DE, ultimately affecting the deposit properties through a variation in tamping. The characterisation of the tamping effect of the coatings sprayed using these various powders, performed through residual stress measurements, is considered for future experiments in order to gain a further understanding of the deposition mechanisms.

The densification mechanism through tamping also characterised by Jenkins et al. on pure Al cold spray deposits was however not observed at higher particle velocities [44]. By spraying powder particles using He and reaching these higher velocities, it is believed that the higher ductility of the as-quenched powder would then lead to a higher quality coating which will be less limited and influenced by the tamping effect of the rebounding particles.

5. Conclusions

For the first time, cold spraying of an Al 7075 powder at different ageing stages was performed. The powders were characterised by SEM and DSC, and the properties of the resulting coatings were tested using ASTM C633 and TCT, combined with microstructural characterisation. The following conclusions were drawn for this study:

- Natural and artificial ageing was performed on a solution heat treated and quenched (SHT + Q) Al 7075 powder leading to a substantial increase in hardness and change of precipitation state, as GP zones and η′ formation were characterised by DSC.

- The ageing process modified the particle-substrate interaction during cold spraying. While the ductility of the SHT + Q powder led to a deformation handled mostly by the particle, the harder, aged powders formed an apparent bonding upon impact highlighted by jetting of the substrate itself.
- Deposition efficiency (DE) and thus the proportion of rebounding particles was found to be a major factor influencing deposit properties as an inverse linear correlation was observed between DE and the cohesion strength of coatings.

CRediT authorship contribution statement

Alexandre Sabard: Conceptualization, Methodology, Investigation, Writing - original draft, Visualization. **Phil McNutt:** Methodology, Supervision. **Henry Begg:** Supervision, Funding acquisition, Resources, Writing - review & editing. **Tanvir Hussain:** Supervision, Funding acquisition, Resources, Writing - review & editing.

Declaration of competing interest

The authors declare that they have no known competing financial interests or personal relationships that could have appeared to influence the work reported in this paper.

Acknowledgement

This work was supported by the Engineering and Physical Sciences Research Council [Grant Number EP/M50810X/1]; in the form of a CASE Ph.D. studentship and industrial funding from TWI via the National Structural Integrity Research Foundation (NSIRC). The authors also acknowledge support from Mr. Damian Whiteman at TWI for conducting the cold spray experiments, and Mr. Daniel Tejero Martín for proof-reading.

References

[1] A.N. Papyrin, A.P. Alkhimov, N.I. Nesterovic, V.F.K. H, M.M. Shushpanov, Gas-dynamic Spraying Method for Applying a Coating, (1990).
[2] H. Assadi, F. Gartner, T. Stoltenhoff, H. Kreye, Bonding mechanism in cold gas spraying, Acta Mater. 51 (2003) 4379–4394, https://doi.org/10.1016/S1359-6454(03)00274-X.
[3] T. Schmidt, F. Gärtner, H. Assadi, H. Kreye, Development of a generalized parameter window for cold spray deposition, Acta Mater. 54 (2006) 729–742, https://doi.org/10.1016/j.actamat.2005.10.005.
[4] T. Schmidt, H. Assadi, F. Gärtner, H. Richter, T. Stoltenhoff, H. Kreye, T. Klassen, From particle acceleration to impact and bonding in cold spraying, J. Therm. Spray Technol. 18 (2009) 794–808, https://doi.org/10.1007/s11666-009-9357-7.
[5] V. Champagne, D. Helfritch, Critical assessment 11: structural repairs by cold spray, Mater. Sci. Technol. 31 (2014) 627–634, https://doi.org/10.1179/1743284714y.0000000723.
[6] S. Yin, P. Cavaliere, B. Aldwell, R. Jenkins, H. Liao, W. Li, R. Lupoi, Cold spray additive manufacturing and repair: fundamentals and applications, Addit. Manuf. 21 (2018) 628–650, https://doi.org/10.1016/j.addma.2018.04.017.
[7] V.K. Champagne, The repair of magnesium rotorcraft components by cold spray, J. Fail. Anal. Prev. 8 (2008) 164–175, https://doi.org/10.1007/s11668-008-9116-y.
[8] J. Villafuerte, Modern cold spray: materials, process, and applications, n.d. https://books.google.co.uk/books?id=afFrCgAAQBAJ&pg=PA352&lpg=PA352&dq=cold+spray+hydraulic+line&source=bl&ots=9mL63mhRyx&sig=ACfU3U0sFbvtof5TF3MOkVlKVS1Oa3OqZw&hl=en&sa=X&ved=2ahUKEwjV1JKPlY_kAhUNXRUIHTMbBosQ6AEwD3oECAgQAQ#v=onepage&q=cold spray hydraulic line&f=false (accessed August 19, 2019).
[9] M. Faccoli, G. Cornacchia, D. Maestrini, G.P. Marconi, R. Roberti, Cold spray repair of martensitic stainless steel components, J. Therm. Spray Technol. 23 (2014) 1270–1280, https://doi.org/10.1007/s11666-014-0129-7.
[10] M.R. Rokni, C.A. Widener, V.K. Champagne, G.A. Crawford, Microstructure and mechanical properties of cold sprayed 7075 deposition during non-isothermal annealing, Surf. Coat. Technol. 276 (2015) 305–315, https://doi.org/10.1016/j.surfcoat.2015.07.016.
[11] M.R. Rokni, C.A. Widener, O.C. Ozdemir, G.A. Crawford, Microstructure and mechanical properties of cold sprayed 6061 Al in As-sprayed and heat treated condition, Surf. Coatings Technol. 309 (2017) 641–650, https://doi.org/10.1016/j.surfcoat.2016.12.035.
[12] A. Sabard, H.L. de Villiers Lovelock, T. Hussain, Microstructural evolution in solution heat treatment of gas-atomized Al alloy (7075) powder for cold spray, J. Therm. Spray Technol. 27 (2018) 145–158, https://doi.org/10.1007/s11666-017-0662-2.
[13] A. Sabard, T. Hussain, Inter-particle bonding in cold spray deposition of a gas-atomised and a solution heat-treated Al 6061 powder, J. Mater. Sci. 54 (2019) 12061–12078, https://doi.org/10.1007/s10853-019-03736-w.
[14] W.A. Story, L.N. Brewer, Heat treatment of gas-atomized powders for cold spray deposition, Metall. Mater. Trans. A Phys. Metall. Mater. Sci. 49 (2018) 446–449, https://doi.org/10.1007/s11661-017-4428-8.
[15] T. Liu, W.A. Story, L.N. Brewer, Effect of heat treatment on the Al-Cu feedstock powders for cold spray deposition, Metall. Mater. Trans. A. 50 (2019) 3373–3387, https://doi.org/10.1007/s11661-019-05230-z.
[16] M.R. Rokni, A.T. Nardi, V.K. Champagne, S.R. Nutt, Effects of preprocessing on multi-direction properties of aluminum alloy cold-spray deposits, J. Therm. Spray Technol. 27 (2018) 818–826, https://doi.org/10.1007/s11666-018-0723-1.
[17] J.E. Hatch, Aluminum Properties and Physical Metallurgy, ASM International, 1984, https://doi.org/10.1361/appm1984p001.
[18] ASM Internationl, Metallurgy of heat treatment and general principles of precipitation hardening, Alum. Prop. Phys. Metall, 1984, pp. 134–199, , https://doi.org/10.1361/appm1984p134.
[19] ASM International. Handbook Committee, Heat treating of aluminium alloys, ASM Handb. Heat Treat, ASM International, 1991, pp. 841–850.
[20] G. Sha, A. Cerezo, Early-stage precipitation in Al-Zn-Mg-Cu alloy (7050), Acta Mater. 52 (2004) 4503–4516, https://doi.org/10.1016/j.actamat.2004.06.025.
[21] L.K. Berg, J. Gjønnes, V. Hansen, X.Z. Li, M. Knutson-Wedel, G. Waterloo, D. Schryvers, L.R. Wallenberg, GP-zones in Al-Zn-Mg alloys and their role in artificial ageing, Acta Mater. 49 (2001) 3443–3451, https://doi.org/10.1016/S1359-6454(01)00251-8.
[22] Y. Zhang, N. Brodusch, S. Descartes, J.M. Shockley, R. Gauvin, R.R. Chromik, The effect of submicron second-phase particles on the rate of grain refinement in a copper-oxygen alloy during cold spray, J. Therm. Spray Technol. 26 (2017) 1509–1516, https://doi.org/10.1007/s11666-017-0603-0.
[23] C. Walde, D. Cote, V. Champagne, R. Sisson, Characterizing the effect of thermal processing on feedstock Al alloy powder for additive manufacturing applications, J. Mater. Eng. Perform. 28 (2019) 601–610, https://doi.org/10.1007/s11665-018-3550-0.
[24] K. Tsaknopoulos, C. Walde, V. Champagne, D. Cote, Gas-atomized Al 6061 powder: phase identification and evolution during thermal treatment, Jom 71 (2019) 435–443, https://doi.org/10.1007/s11837-018-3175-7.
[25] S. Vijayan, B.A. Bedard, M.A. Gleason, H.R. Leonard, D.L. Cote, M. Aindow, Studies of thermally activated processes in gas-atomized Al alloy powders: in situ STEM heating experiments on FIB-cut cross sections, J. Mater. Sci. 54 (2019) 9921–9932, https://doi.org/10.1007/s10853-019-03562-0.
[26] T. Schmidt, F. Gaertner, H. Kreye, New Developments in Cold Spray Based on Higher Gas and Particle Temperatures, (n.d.). doi:https://doi.org/10.1361/105996306X147144.
[27] ASTM International, ASTM C633-01 Standard Test Method for Adhesion of Cohesion Strength of Thermal Spray Coatings, (2001).
[28] D.J. Lloyd, M.C. Chaturvedi, A calorimetric study of aluminium alloy AA-7075, J. Mater. Sci. 17 (1982) 1819–1824, https://doi.org/10.1007/BF00540811.
[29] C. Garda-Cordovilla, E. Louis, Communications kinetics of retrogression in AI-Zn-Mg-(Cu) alloys, n.d. https://link.springer.com/content/pdf/10.1007%2FBF02647890.pdf (accessed August 15, 2019).
[30] X.J. Jiang, J. Tafto, B. Noble, B. Holme, G. Waterloo, Differential Scanning Calorimetry and Electron Diffraction Investigation on Low-temperature Aging in Al-Zn-Mg Alloys, (2007), https://doi.org/10.1007/s11661-000-0269-x.
[31] X.M. Li, M.J. Starink, DSC study on phase transitions and their correlation with properties of Overaged Al-Zn-Mg-Cu alloys, J. Mater. Eng. Perform. 21 (2012) 977–984, https://doi.org/10.1007/s11665-011-9973-5.
[32] R. Deiasi, P.N. Adler, Calorimetric studies of 7000 series aluminum alloys: I. Matrix precipitate characterization of 7075, n.d. https://link.springer.com/content/pdf/10.1007%2FBF02667403.pdf (accessed August 8, 2019).
[33] J. Lendvai, G. Honyek, I. Kovács, Dissolution of second phases in an Al–Zn–Mg alloy investigated by calorimetric method, Scr. Metall. 13 (1979) 593–594, https://doi.org/10.1016/0036-9748(79)90115-7.
[34] H. Herman, J.B. Cohen, M.E. Fine, Formation and reversion of Guinier-Preston zones in Al-5.3 at.% Zn, Acta Metall. 11 (1963) 43–56, https://doi.org/10.1016/0001-6160(63)90123-8.
[35] A.K. Mukhopadhyay, K.S. Prasad, Formation of plate-shaped Guinier–Preston zones during natural aging of an Al–Zn–Mg–Cu–Zr alloy, Philos. Mag. Lett. 91 (2011) 214–222, https://doi.org/10.1080/09500839.2010.547525.
[36] J.E. Hatch, Microstructure of alloys*, in: J.E. Hatch (Ed.), Alum. Prop. Phys. Metall, ASM International, 1984, pp. 58–104, , https://doi.org/10.1361/appm1984p058.
[37] G.E. Totten, D.S. MacKenzie, Handbook of Aluminium, Volume 1: Physical Metallurgy and Processes, 7 CRC Press, New York, 2003, pp. 121–123 https://books.google.co.uk/books?id=Wbwv3nt1gp0C&pg=PA288&lpg=PA288&dq=Al+zn+mg+cu+aging&source=bl&ots=HuT8J48FuH&sig=fVSMUwwyT2xkoxFz_7oHTlGAJR0&hl=fr&sa=X&ved=0ahUKEwiAvbG4-bzQAhUlBMAKHYVfC2sQ6AEIbDAI#v=onepage&q=Alznmgcuaging&f=false.
[38] C.J. Kong, P.D. Brown, S.J. Harris, D.G. McCartney, Analysis of microstructure formation in gas-atomised Al-12 wt.% Sn-1 wt.% Cu alloy powder, Mater. Sci. Eng. A 454–455 (2007) 252–259, https://doi.org/10.1016/j.msea.2006.11.050.
[39] V.S. Bhattiprolu, K.W. Johnson, O.C. Ozdemir, G.A. Crawford, Influence of feedstock powder and cold spray processing parameters on microstructure and mechanical properties of Ti-6Al-4V cold spray depositions, Surf. Coatings Technol. 335 (2018) 1–12, https://doi.org/10.1016/J.SURFCOAT.2017.12.014.
[40] J. Tang, Z. Zhao, N. Li, X. Qiu, Y. Shen, X. Cui, H. Du, J. Wang, T. Xiong, Influence of feedstock powder on microstructure and mechanical properties of Ta cold spray

depositions, Surf. Coatings Technol. 377 (2019) 124903, , https://doi.org/10.1016/J.SURFCOAT.2019.124903.
[41] L.N. Brewer, J.F. Schiel, E.S.K. Menon, D.J. Woo, The connections between powder variability and coating microstructures for cold spray deposition of austenitic stainless steel, Surf. Coatings Technol. 334 (2018) 50–60, https://doi.org/10.1016/J.SURFCOAT.2017.10.082.
[42] W. Yang, S. Ji, M. Wang, Z. Li, Precipitation behaviour of Al–Zn–Mg–Cu alloy and diffraction analysis from η′ precipitates in four variants, J. Alloys Compd. 610 (2014) 623–629, https://doi.org/10.1016/J.JALLCOM.2014.05.061.
[43] G. Bae, Y. Xiong, S. Kumar, K. Kang, C. Lee, General aspects of interface bonding in kinetic sprayed coatings, Acta Mater. 56 (2008) 4858–4868, https://doi.org/10.1016/j.actamat.2008.06.003.
[44] R. Jenkins, S. Yin, B. Aldwell, M. Meyer, R. Lupoi, New insights into the in-process densification mechanism of cold spray Al coatings: low deposition efficiency induced densification, J. Mater. Sci. Technol. 35 (2019) 427–431, https://doi.org/10.1016/J.JMST.2018.09.045.